IEEE Access
Multidisciplinary ⋮ Rapid Review ⋮ Open Access Journal

Received January 22, 2022, accepted February 8, 2022, date of publication February 11, 2022, date of current version February 22, 2022.

Digital Object Identifier 10.1109/ACCESS.2022.3151163

Surface-Impedance Formulation for Hollow-Core Waveguides Based on Subwavelength Gratings

ANGELA COVES[1], (Senior Member, IEEE), HAROLDO MAESTRE[1], RAIMON ARCHILÉS[2], MIGUEL V. ANDRÉS[2], (Senior Member, IEEE), AND BENITO GIMENO[3], (Member, IEEE)

[1]Department of Communications Engineering-I3E, Universidad Miguel Hernández de Elche, 03202 Elche, Spain
[2]Department of Applied Physics and Electromagnetism-ICMUV, Universidad de Valencia, 46100 Burjasot, Valencia, Spain
[3]Department of Applied Physics and Electromagnetism, IFIC (CSIC-University of Valencia), 46100 Burjasot, Valencia, Spain

Corresponding author: Angela Coves (angela.coves@umh.es)

The work of Angela Coves was supported in part by the Ministerio de Ciencia e Innovación (MCIN)/Agencia Estatal de Investigación (AEI)/10.13039/501100011033 under Grant PID2019-103982RB-C43, and in part by the European Union "European Regional Development Fund (ERDF) A way of making Europe." The work of Miguel V. Andrés was supported in part by MCIN/AEI/10.13039/501100011033 under Grant PDI2019-104276RB-I00, in part by the European Union "ERDF A way of making Europe," and in part by the Generalitat Valenciana under Grant PROMETEO/2019/048.

ABSTRACT A rigorous Surface Impedance (SI) formulation for planar waveguides is presented. This modal technique splits the modal analysis of the waveguide in two steps. First, we obtain the modes characteristic equations as a function of the SI and, second, we need to obtain the surface impedance values using either analytical or numerical methods. We validate the technique by comparison with well-known analytical cases: the parallel-plate waveguide with losses and the dielectric slab waveguide. Then, we analyze an optical hollow-core waveguide defined by two high-contrast subwavelength gratings validating our results by comparison with reported values. Finally, we show the potential of our formulation with the analysis of a THz hollow-core waveguide defined by two surface-relief subwavelength gratings, including material losses in our formulation.

INDEX TERMS Surface impedance, hollow-core waveguide, surface-relief grating.

I. INTRODUCTION

Waveguides with special microstructured boundaries are being proposed to improve guidance of electromagnetic waves, particularly in the frequency ranges where materials' absorption is a critical drawback. The interest on the design and fabrication of THz waveguides is continuously growing in the last years [1]. THz waveguides can benefit from the use of gratings [2], antiresonant [3] and bandgap [4] effects. Thus, attenuation and dispersion properties of hollow-core waveguides with microstructured boundaries have been investigated with different geometries, materials and numerical methods [5]– [8]. Among the theoretical tools that are being used for the simulation of THz waveguides we can point out the analytical methods [3], [5] based on some basic ray-optics approximations and the pure numerical approaches based on vector finite element methods [9]. On the other hand, commercial electromagnetic simulators (for instance [10], [11]) have the tools to fully analyze these waveguide structures. However, in hollow-core waveguides with microstructured boundaries and large transverse dimension, the needed run-time may be considerable on the one hand, and on the other hand, their driven modal solvers provide the first propagating modes of the waveguide, which requires a huge amount of memory (there are a great number of solutions which are bounded to the dielectric waveguide walls), and they are not well suited for analyzing the low-loss propagating mode in the air region of such waveguides. By contrast, the eigenmode solvers in these packages are much faster but they provide systematically the frequency behavior of only the real part of the complex propagation factor (an eigenvalue problem is defined by imposing a given phase shift between the boundaries of the unit cell, and the corresponding eigenfrequency is then computed [12]), and thus, the attenuation constant in this kind of hollow-core waveguides with microstructured boundaries cannot be obtained with such electromagnetic simulators.

The main contribution is summarized as follows.

1) Here we propose a modal approach for the modelling of planar waveguides in which the walls that define the core of the waveguide are described in terms of the surface impedance (SI). This technique is inspired by the most

The associate editor coordinating the review of this manuscript and approving it for publication was Guido Valerio.

basic impedance matching methods [13] and the concept of SI [14]. Our approach follows a generalization of the surface impedance method, and is fully rigorous provided that we have an accurate knowledge of the SI. We propose to solve frequency domain Maxwell equations, in order to obtain the modes of the planar waveguide, in two steps. First we will write the characteristic equations for the modes of planar waveguides in terms of the SI. Then, in a second step, we will need to provide the actual values of the SI in order to obtain the propagation constant of the modes. Depending on the particular problem, we might be able to provide analytical expressions for the SI. Alternatively, we will require a numerical technique to obtain the SI values, which is rather simpler than trying to solve the modes of the waveguide directly. In addition, by splitting the problem in two steps we can gain some important physical insights.

2) There are already previous more rigorous methods for the analysis and application in design of hollow-core THz dielectric waveguides with certain simple configurations, like the one in [3], consisting of dielectric tube waveguides with absorptive cladding, or like photonic crystal-based hollow-core waveguides [15], all of them showing an important difference to the one analyzed in our work, which is the translational symmetry of such waveguide configurations. Although different rigorous methods can be applied for analyzing such type of hollow-core waveguides with translational symmetry, they show a waveguide loss which is typically two orders of magnitude higher than that proposed in this work because the field penetration depth in such hollow-core waveguides is significantly higher, and consequently, its attenuation loss factor gets increased. Alternatively, the use of a hollow-core waveguide with special microstructured boundaries along the propagation direction is proposed here to improve guidance of electromagnetic waves in a frequency range where materials' absorption is a critical drawback, like at THz frequencies, whose design is based on high reflectivity gratings constituting the waveguide walls (there are many works based on different methods that can be employed to this end, like the well-known coupled wave analysis, or the modal method employed in this work [16]). Nevertheless, to the knowledge of the authors, the rigorous calculation of the waveguide loss in this type of sub-wavelength HCG-HW has not been previously done. While rigorous methods have been recently developed for computing the dispersion diagrams of periodic guiding structures with different unit cell configurations [17], [18], whose analysis procedure systematically provides their first Floquet propagating modes, they are not well suited for analyzing the low-loss propagating mode we are interested in of the proposed waveguide. The reason is because there are a great deal of solutions which are bounded to the dielectric waveguide walls, which will appear before the one we are interested in, because they have a higher propagation constant, so this is not an easy task, and most of all, it is not as straightforward as in the proposed technique in this work.

3) The proposed method presents an important contribution to the analysis and design of hollow-core waveguides formed by lossy dielectric gratings, and especially, to the calculation of their propagation loss, which has not been previously published. The use of a vectorial modal method in combination with a novel developed surface impedance formulation, allows to rigorously obtain the complex propagation factor of the fundamental mode propagating in this kind of waveguides (including not only the reflection losses but also the dielectric losses of the grating materials). This has not been done in previous works that have analyzed similar waveguides in the optical regime (e.g., in [5], [6]), whose techniques use some basic ray-optics approximations based on the computation of the power reflection coefficient on the gratings constituting the waveguide walls, being thus limited to lossless dielectric materials (this fundamental limitation is discussed for example in [19]). Such limitation, which is not important at optical wavelengths, where dielectric losses can be negligible, cannot be ignored at THz frequencies, where dielectric losses are higher.

The proposed technique has been formulated for a guiding structure which is invariant along the $z-$ and $y-$axes. In order to extend the SI formulation to the case of a guiding structure with periodicity along the $z-$axis and invariant along the $y-$axis, in the most general case, it would be required to expand the fields in terms of N Floquet orders, making the SI matrix formulation unapproachable. For this reason, in this paper, the proposed technique has been restricted to the modelling of planar waveguides with microstructured boundaries, which is the problem with practical interest, in which the periodicity of the structure is subwavelength, i. e., for zero-th order gratings, in which case, the SI can be represented by a 2×2 matrix. The subwavelength period restriction affects the SI formulation, although the periodic nature of the gratings constituting the planar waveguide has been rigorously considered in the analysis of the dispersion characteristics of the gratings, as fully explained in [16].

After this introduction, we will develop in detail the theoretical formulation for the modes characteristic equations of planar waveguides in terms of the SI. Then, we will illustrate how the method is applied for two basic cases in which analytical expressions for the SI are available: (a) parallel-plate waveguide defined by good conductors and (b) dielectric slab waveguide. This will provide a first validation of the proposed formulation. Next, we will apply our approach to a hollow-core slab THz waveguide defined by two subwavelength gratings. In this case, since the SI values are obtained numerically, we will require to implement an iterative method. Our technique will be validated by comparison with the numerical results published previously by other authors that use alternative techniques. Finally, we will conclude and highlight the advantages and new possibilities provided by our technique. It is worthwhile to point out that although we will consider here only planar waveguides, our approach could be extended to cylindrical waveguides following the fundamentals developed in [14].

II. SURFACE IMPEDANCE FORMULATION IN A PLANAR WAVEGUIDE

In this work we present a generalization of the concept of surface impedance of planar boundaries by means of a second-order tensor magnitude, which is called surface impedance [14]. As we will briefly show, the SI technique accurately provides the characteristic equations for planar waveguides formed by conductor-dielectric and dielectric-dielectric planar interfaces considering losses. Thus, this formulation can be extended to analyze waveguides with periodic micro-structured surfaces or subwavelength grating interfaces, as it will be shown.

We begin our analysis with the definition, in Fig. 1, of the waveguide geometry which will be used throughout the text. The planar waveguide is formed by a homogeneous medium of dielectric permittivity ε_1, magnetic permeability μ_1 and thickness a, surrounded by an external homogeneous medium, and in which the upper and bottom boundaries have planar symmetry. The $z-$axis corresponds to the propagation direction, while the $x-$axis is perpendicular to the waveguide boundaries, and the $y-$axis is parallel to the boundaries.

The fields of the modes will be written in the conventional form:

$$\mathbf{E}(x,z,t) = \left[e_x(x)\mathbf{u}_x + e_y(x)\mathbf{u}_y + e_z(x)\mathbf{u}_z\right] e^{j(\omega t-\beta z)} \quad (1)$$

$$\mathbf{H}(x,z,t) = \left[h_x(x)\mathbf{u}_x + h_y(x)\mathbf{u}_y + h_z(x)\mathbf{u}_z\right] e^{j(\omega t-\beta z)} \quad (2)$$

where $j = \sqrt{-1}$ is the imaginary unit, the functions e_x, e_y, e_z determine the field components of the electric field, the functions h_x, h_y, h_z determine the field components of the magnetic field, β is the complex propagation factor, and ω is the angular frequency.

The tangential field components of the guided modes in the waveguide boundaries ($x = \pm a/2$) satisfy the following boundary conditions [14]:

$$\mathbf{E}_t = j\overline{\boldsymbol{\chi}} \cdot (\mathbf{u} \times \mathbf{H}_t) \quad (3)$$

where $\mathbf{E}_t$ and $\mathbf{H}_t$ are, respectively, the electric and magnetic field components tangential to the interfaces, $\mathbf{u}$ is a unit vector normal to the interfaces, pointing outwards the waveguide, and $\overline{\boldsymbol{\chi}}$ is a tensor called the SI, which can be written as:

$$\overline{\boldsymbol{\chi}} = \begin{pmatrix} \chi_{11} & \chi_{12} \\ \chi_{21} & \chi_{22} \end{pmatrix}. \quad (4)$$

In this analysis, only the tangential field components are needed to satisfy the boundary conditions given by (3). For a planar waveguide, such tangential field components are:

$$e_z = A\sin(k_x x) + B\cos(k_x x) \quad (5a)$$

$$h_z = C\sin(k_x x) + D\cos(k_x x) \quad (5b)$$

$$e_y = ((j\omega\mu_1)/k_x)[C\cos(k_x x) - D\sin(k_x x)] \quad (5c)$$

$$h_y = ((-j\omega\varepsilon_1)/k_x)[A\cos(k_x x) - B\sin(k_x x)] \quad (5d)$$

$$-a/2 < x < a/2$$

where A, B, C and D are constants, and k_x is the transverse propagation factor.

Taking into account the geometry defined in Fig. 1 and (5a-5d), (3) can thus be rewritten as:

$$\left[\begin{pmatrix} e_y \\ e_z \end{pmatrix} = j\begin{pmatrix} \chi_{11} & \chi_{12} \\ \chi_{21} & \chi_{22} \end{pmatrix}\begin{pmatrix} \mp h_z \\ \pm h_y \end{pmatrix}\right]_{x=\pm a/2}, \quad (6)$$

where $\mathbf{u} = \pm\mathbf{u}_x$ at $\pm a/2$. We can substitute (5a-5d) into (6), which yields a new set of four equations which can be solved as a system of linear equations considering coefficients A, B, C and D in (5) as the system unknowns. In order to have a solution other than the trivial one ($A = B = C = D = 0$), its determinant must be zero, which yields the characteristic equations of a planar waveguide in terms of the SI elements, whose expressions can be found in the Appendix. Moreover, this set of equations determine the field components by expressing, for example, the coefficients B, C and D as a function of the coefficient A. In the presence of the off-diagonal elements in the SI tensor, the obtained modes are the well-known E-type and H-type modes [20], which correspond to off-plane (out of the xz plane) propagation, also called conical incidence.

In the following, the cases that are discussed can be described in a simplified framework in which χ_{12} and χ_{21} are zero. However, we find interesting to give the general formulation, having in mind future developments to deal with rectangular cross section waveguides, as well as inhomogeneous waveguides, in which all four coefficients are likely to be non-zero.

These expressions give the characteristic equations of the well-known TM and TE modes when $\chi_{12} = \chi_{21} = 0$, after a simple analysis of the above mentioned system of four equations. In particular, TM modes require $h_z = 0$ (i. e., $C = D = 0$), thus $e_y = 0$ (see (5c)), and, according to (6), χ_{12} must be zero since h_y will have to be different from zero. Additionally, TE modes require $e_z = 0$ (i. e., $A = B = 0$), thus $h_y = 0$ (see (5d)), and, according to (6), χ_{21} must be zero since h_z will have to be different from zero. The characteristic equation for the symmetric TM (TM_S) modes, with $h_z = 0$, $e_z = A\sin(k_x x)$, and $B = C = D = 0$, and for the antisymmetric TM (TM_A) modes with $h_z = 0$, $e_z = B\cos(k_x x)$, and $A = C = D = 0$, are derived from (A.34, A.35), respectively:

$$TM_S \Rightarrow (\chi_{22}\omega\varepsilon_1)/k_x = \tan(k_x a/2) \quad (7a)$$

$$TM_A \Rightarrow (\chi_{22}\omega\varepsilon_1)/k_x = -\cot(k_x a/2) \quad (7b)$$

while the characteristic equation for the symmetric TE (TE_S) modes, with $e_z = 0$, $h_z = C\sin(k_x x)$, and $A = B = D = 0$, and for the antisymmetric TE (TE_A) modes with $e_z = 0$, $h_z = D\cos(k_x x)$, and $A = B = C = 0$, are derived from (A.36, A.37), respectively:

$$TE_S \Rightarrow (\chi_{11}k_x)/(\omega\mu_1) = -\cot(k_x a/2) \quad (8a)$$

$$TE_A \Rightarrow (\chi_{11}k_x)/(\omega\mu_1) = \tan(k_x(a/2). \quad (8b)$$

It should be mentioned that a given mode is classified as symmetric or antisymmetric depending on the symmetry of

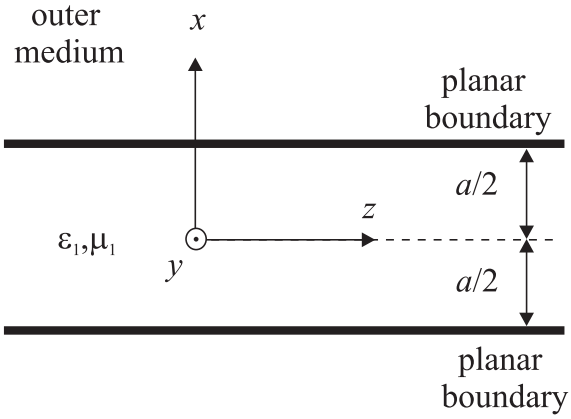

FIGURE 1. Schematic of a waveguide with planar symmetry.

the transverse field component, h_y and e_y for the TM and the TE modes, respectively.

Next, in order to validate the obtained set of characteristic equations (7a)-(8b), we will apply the SI approach to some examples of planar waveguide structures with well-known analytical solution. In particular, we will study a parallel-plate waveguide and a dielectric slab waveguide.

A. PARALLEL-PLATE WAVEGUIDE

Here it is shown how the SI concept provides the characteristic equations of the TE and TM modes of the parallel-plate waveguide with finite conductivity, whose propagation region of permittivity ε is delimited by two parallel metallic sheets separated by a fixed distance a (the perfect conductor case can be derived as a particular solution by imposing infinite conductivity on the metallic sheets).

In this case, the procedure is straightforward. We only have to write the surface impedance tensor $\overline{\chi}$ in terms of the surface impedance of a good conductor (Z_S) which is determined by the Leontovich boundary condition [21]:

$$\mathbf{E}_t = Z_S(\mathbf{n} \times \mathbf{H}_t) \tag{9}$$

where $\mathbf{n}$ is a unitary vector, normal to the surface of the conductor and pointing outwards the conductor (in our case: $\mathbf{n} = -\mathbf{u}$, and Z_S is the conductor characteristic impedance, given by the expression:

$$Z_S = (1+j)\sqrt{\frac{\omega\mu}{2\sigma}} \tag{10}$$

where μ and σ are the magnetic permeability and the electric conductivity of the conductor, respectively. Rewriting (9) in the form of (6), we find the actual value of $\overline{\chi}$ in the case of the parallel-plate waveguide:

$$\chi_{11} = \chi_{22} = jZ_S \quad \chi_{12} = \chi_{21} = 0 \tag{11}$$

Being $\chi_{12} = \chi_{21} = 0$, we can confirm that the solution splits into the two families of TM and TE modes. In addition, taking into account the actual values of χ_{11} and χ_{22}, we obtain the characteristic equations for the TM and TE modes of the parallel-plate waveguide:

$$\mathrm{TM}_S \Rightarrow (jZ_S\omega\varepsilon_1)/(k_x) = \tan((k_x a)/2) \tag{12a}$$
$$\mathrm{TM}_A \Rightarrow (jZ_S\omega\varepsilon_1)/k_x = -\cot(k_x a/2) \tag{12b}$$
$$\mathrm{TE}_S \Rightarrow (jZ_S k_x)/(\omega\mu_1) = -\cot(k_x a/2) \tag{13a}$$
$$\mathrm{TE}_A \Rightarrow (jZ_S k_x)/(\omega\mu_1) = \tan(k_x a/2) \tag{13b}$$

In the case of perfect conductors plates, $Z_S = 0$, so we obtain the expected values for the transverse and axial propagation factors ($k_{x0,m}$ and $\beta_{0,m}$) of TM_m and TE_m modes

$$k_{x0,m} = \frac{\pi m}{a} \;\rightarrow\; \beta_{0,m} = \sqrt{k^2 - k_{x0,m}^2} \tag{14}$$

where $m > 0$: the odd values of m correspond to the TM_A and TE_S modes, and the even values to the TM_S and TE_A modes.

In the case of good conductor plates, we can obtain a first order approximation for the transverse and axial propagation factors ($k_{x,m}$ and β_m), using (12-13) and assuming that the actual value of Z_S will be extremely small:

$$\mathrm{TM}_m \Rightarrow k_{x,m} = k_{x0,m} + (j2\omega\varepsilon_1 Z_S)/(ak_{x0,m}),$$
$$\beta_m = \beta_{0,m} - (j2\omega\varepsilon_1 Z_S)/(a\beta_{0,m}) \tag{15}$$
$$\mathrm{TE}_m \Rightarrow k_{x,m} = k_{x0,m} + (j2k_{x0,m}Z_S)/(a\omega\mu_1),$$
$$\beta_m = \beta_{0,m} - (j2k_{x0,m}^2 Z_S)/(a\omega\mu_1\beta_{0,m}) \tag{16}$$

The above first order approximations for β_m only apply far away from the cut-off frequency, when $\beta_{0,m} \neq 0$. Thus, the real part of Z_S will determine the imaginary part of β_m, i. e., the attenuation coefficient, while the imaginary part of Z_S gives a small correction of the real part which is mainly determined by $\beta_{0,m}$. The analytical expression of the attenuation coefficient α_m is:

$$\mathrm{TM}_m \Rightarrow \alpha_m = (2\omega\varepsilon)/(a\beta_{0,m})\sqrt{(\omega\mu)/(2\sigma)} \tag{17}$$
$$\mathrm{TE}_m \Rightarrow \alpha_m = (2k_{x0,m}^2)/(a\omega\mu\beta_{0,m})\sqrt{(\omega\mu)/(2\sigma)} \tag{18}$$

Exactly the same expressions are obtained by calculating the losses in the conductors and the total power flux with the fields of the ideal case, following the conventional perturbative technique [21].

B. DIELECTRIC SLAB WAVEGUIDE

In the dielectric slab waveguide, the propagation region, characterized by its permittivity ε_1 is delimited by two dielectric frontiers separated by a fixed distance a, each of which is a planar interface between two dielectric regions. In order to derive the expressions for the SI of these interfaces, we recall the incidence of a plane wave on the interface. In Fig. 2(a) it is represented the geometry of a plane wave incident on a dielectric interface for the TM case, and in Fig. 2(b) for the TE case, respectively.

From Fig. 2(a), the continuity equations for the TM incidence at the interface, for the electric and magnetic fields, can be expressed as:

$$E_{1z} = E_{iz} + E_{rz} = E_{2z} \tag{19a}$$
$$H_{1y} = H_{iy} + H_{ry} = H_{2y} \tag{19b}$$

where the sub-index i and r depict incidence and reflection, respectively. The surface impedance can thus be defined as the ratio of the non zero electric and magnetic field tangential components at either side of the interface:

$$Z^{TM} = \frac{E_{1z}}{H_{1y}} = \frac{E_{2z}}{H_{2y}} = \eta_2 \cos\theta_t \tag{20}$$

where η_2 is the intrinsic impedance of the outer waveguide medium, and θ_t is the transmission angle from medium 1 to medium 2.

Also, from Fig. 2(b), the continuity equations for the TE incidence, for the electric and magnetic fields, can be expressed as:

$$E_{1y} = E_{iy} + E_{ry} = E_{2y} \tag{21a}$$
$$H_{1z} = H_{iz} + H_{rz} = H_{2z}. \tag{21b}$$

Likewise the TM case, the surface impedance can also be defined as the ratio of the non zero electric and magnetic field tangential components at either side of the interface:

$$Z^{TE} = \frac{E_{1z}}{H_{1y}} = \frac{E_{2z}}{H_{2y}} = \frac{\eta_2}{\cos\theta_t}. \tag{22}$$

We can summarize (20) and (22) in the following matrix equation:

$$\left[\begin{pmatrix} E_{1y} \\ E_{1z} \end{pmatrix} = -\begin{pmatrix} Z^{TE} & 0 \\ 0 & Z^{TM} \end{pmatrix}\begin{pmatrix} H_{1z} \\ -H_{1y} \end{pmatrix}\right]_{x=-a/2} \tag{23}$$

where the wave impinges from medium 1 to medium 2 at the lower waveguide boundary. However, the wave can also impinge from medium 1 to medium 2 at the upper waveguide boundary, and thus, (23) becomes:

$$\left[\begin{pmatrix} E_{1y} \\ E_{1z} \end{pmatrix} = -\begin{pmatrix} Z^{TE} & 0 \\ 0 & Z^{TM} \end{pmatrix}\begin{pmatrix} -H_{1z} \\ H_{1y} \end{pmatrix}\right]_{x=+a/2} \tag{24}$$

The comparison of (23) and (24) with (4) permits to derive the values of χ_{ij} for the dielectric interface:

$$\chi_{11} = jZ^{TE}, \quad \chi_{22} = jZ^{TM}, \quad \chi_{12} = \chi_{21} = 0 \tag{25}$$

These values determine the characteristic equations for the TM and TE modes in combination with (5-6). In order to make explicit the dependence of the characteristic equations on the transverse and axial propagation factors, we can rewrite Z^{TE} and Z^{TM} in the form

$$Z^{TM} = \eta_2 \cos\theta_t = (\eta_0\sqrt{1 - [(n_1\beta)/(n_2k_1)]^2})/n_2 \tag{26}$$
$$Z^{TE} = \eta_2/\cos\theta_t = \eta_0/(n_2\sqrt{1 - [(n_1\beta)/(n_2k_1)]^2}) \tag{27}$$

where the impedance of medium 2 has been written as a function of the impedance of vacuum (η_0) and the refractive index (n_2), the transmission angle as a function of the incident angle, and finally the sine of the incident angle as β/k_1, being k_1 the wavenumber in medium 1.

Thus, the characteristic equations (7-8) have the following expressions for the dielectric slab waveguide:

$$\mathrm{TM}_S \Rightarrow \tan((k_x a)/2) = (n_1^2\sqrt{\beta^2 - k_2^2})/(n_2^2 k_x) \tag{28a}$$
$$\mathrm{TM}_A \Rightarrow \cot((k_x a)/2)) = -(n_1^2\sqrt{\beta^2 - k_2^2})/(n_2^2 k_x) \tag{28b}$$
$$\mathrm{TE}_S \Rightarrow \tan((k_x a)/2) = \sqrt{\beta^2 - k_2^2}/k_x \tag{29a}$$
$$\mathrm{TE}_A \Rightarrow \cot((k_x a)/2)) = -\sqrt{\beta^2 - k_2^2}/k_x \tag{29b}$$

where non magnetic dielectrics are assumed ($\mu_1 = \mu_2 = \mu_0$, μ_0 being the magnetic permeability of vacuum), and k_2 is the wavenumber in medium 2. These expressions match exactly the analytic characteristic equations of TE and TM modes of a dielectric slab waveguide, as they are reported in most common waveguide books (see for example [22]).

After this section, in which we have tested the SI formulation with two analytic cases, we move to more complex waveguides with non analytical solution. Now, in the next section, we will study a THz waveguide defined by two subwavelength gratings. In this case only numerical information on the surface impedance will be available.

III. ANALYSIS AND DESIGN OF A HOLLOW-CORE THz WAVEGUIDE BASED ON HIGH-CONTRAST SUBWAVELENGTH GRATINGS

The purpose of this section is to apply the SI formulation described above to the analysis of a particular waveguide with planar symmetry, consisting of a low loss hollow-core THz waveguide structure, and to compare this formulation with the ray-optics approximation. The waveguide under study consists of two reflecting high-index-contrast gratings (HCGs) that are periodic in the z direction and infinite in the y direction, in which the period is subwavelength. The basic principle of this hollow-core waveguide is to guide a THz beam propagating through air by multiple reflections on the HCGs, which act as high reflectivity claddings reflecting waves at a small glancing angle (see Fig. 3). The two HCGs are spaced a distance a apart. This hollow-core waveguide structure was first reported in guided-wave optics [5], showing an exceedingly low propagation loss associated to an ultrahigh reflectivity of the HCGs. In [5], the high-index material employed in the HCGs was a semiconductor with relative permittivity $\varepsilon_r = 12.96$ surrounded by air; material losses were neglected. However, at THz frequencies, the material losses must be rigorously accounted for in order to get accurate results in this waveguide configuration.

In order to obtain the SI of the gratings that define the waveguide, we can compute the reflection coefficient ρ of the HCG for plane wave incidence. This calculation is performed by using the vector modal method that we developed years ago [16]. For example, if we pay attention to the TM and TE incidence, we find that $\rho_{TM,TE}$ defines the surface impedance

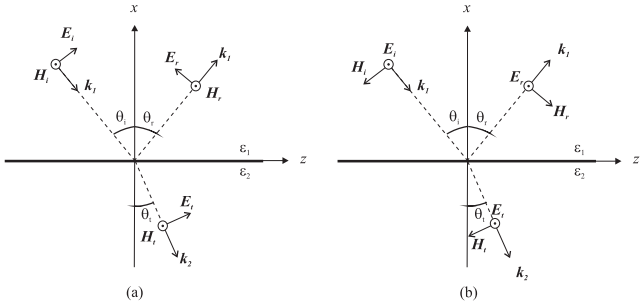

FIGURE 2. Geometry of a plane wave incident on a dielectric interface. a) TM incidence and b) TE incidence.

$Z_S^{TM,TE}$ through the relations [23]:

$$Z_S^{TM} = \eta_1 \cos(\theta_i)[(1+\rho^{TM})/(1-\rho^{TM})] \quad (30)$$

$$Z_S^{TE} = (\eta_1/\cos(\theta_i))[(1+\rho^{TE})/(1-\rho^{TE})] \quad (31)$$

where η_1 is the intrinsic impedance of medium 1 and θ_i is the angle of incidence on the HCG. As in section II.B, the sine of the incident angle is equal to β/k_1. Thus the SI will be determined by the actual values of $Z_S^{TM,TE}$:

$$\chi_{11} = Z_S^{TE}, \quad \chi_{22} = Z_S^{TM}, \quad \chi_{12} = \chi_{21} = 0 \quad (32)$$

Although this result expresses the basic concept that we will exploit for the implementation of the technique by introducing these values in (7)-(8), we need to go a step further. Material absorption in the THz range of frequencies is not usually negligible. Moreover, radiation losses in a waveguide as that depicted in Fig. 3 are not negligible either. Therefore, we need to consider that the propagation factor β will be complex, which is equivalent to say that the incident angle θ_i will be also complex. This is not a limitation for our approach, since we can compute the field components that define $Z_S^{TM,TE}$ without any intrinsic restriction, as it was demonstrated in [16]. However, other techniques that require computing the power reflection coefficient might find fundamental limitations when trying to include lossy materials, as it happens with the technique reported in [5]. These fundamental limitations are discussed for example in [19] (chapter 2 Basic Theory, section The Simple Boundary, subsection Normal Incidence in Absorbing Media), and are also the reason for the operator governing the propagation of electromagnetic waves in waveguides with lossy dielectrics to be nonself-adjoint [24]. To this end, in the next sub-section, an iterative method combined with the SI formulation is described for the rigorous calculation of the complex propagating factor $\beta - \mathrm{i}$. e., including losses - in this waveguide.

A. DESCRIPTION OF THE ITERATIVE METHOD

In order to obtain the modes of the proposed hollow-core waveguide, we have to solve the characteristic equations in which the SI coefficients are an implicit function of the propagation factor, which has to be numerically solved. We propose an iterative method, and we will take as the 0-th iteration solution the modes of the ideal parallel-plate waveguide (without losses). If we use the superscript (n) to indicate the iteration order, we will take $k_x^{(0)}$ and $\beta^{(0)}$ equal to the values given by (14). This 0-th iteration corresponds to the angle of incidence $\theta_i^{(0)}$, being $\sin(\theta_i^{(0)}) = \beta^{(0)}/k_1$. This method can be applied to obtain the different m-order modes in the hollow-core waveguide. In the following, we will apply the iterative method to obtain the first TE mode (m = 1 in (14)), given that we have chosen the grating parameters such that the high reflectivity is only achieved at glancing angles and TE polarization, which corresponds to the first TE propagative mode. The iterative method is still valid for obtaining non-glancing higher order modes present in the structure, but it will be poorly convergent in this case. However, we are not interested in them, because they will be effectively filtered out due to their high reflection losses.

In this 0-th iteration, both $k_x^{(0)}$ and $\beta^{(0)}$ are real, and thus the incident angle $\theta_i^{(0)}$ is real. Then, in the next iterations of n order, following the analysis described above for obtaining the modes in a waveguide with planar symmetry, the TE symmetric characteristic equation (see (8a)) in our waveguide must be numerically solved (i.e., the value of $k_x^{(n)}$). To this end, the value of the incident angle $\theta_i^{(n-1)}$, which in general will be complex, has been used to compute the complex reflection coefficient $\rho^{(n)}$ in the inner face of the hollow-core waveguide, following the vector modal method developed in [16]. This reflection coefficient can be related to the TE surface impedance Z_s^{TE} by using (31), and thus, to the first element of the surface impedance tensor $\chi_{11} = jZ_s^{TE}$ appearing in (8a). Finally, the numerical solution of (8a) yields $k_x^{(n)}$, and from its value, $\theta_i^{(n)}$, and also $\beta^{(n)}$:

$$\beta^{(n)} = \sqrt{k_0^2 - \left(k_x^{(n)}\right)} \quad (33)$$

whose imaginary part is directly related to the attenuation coefficient $\alpha^{(n)}$ (Np/m) of the waveguide in the n-th iteration. The iterative process finishes once convergence is reached.

B. COMPARISON WITH RESULTS REPORTED IN THE TECHNICAL LITERATURE

In order to check the validity of the proposed iterative analysis method, we have first compared the propagation loss of a waveguide with planar symmetry with results presented in the technical literature. We have analyzed an optical ultra-low loss single-mode hollow-core waveguide using subwavelength HCGs, which was proposed in [5] for guided-wave optics, with a core size a of 15 μm (corresponding to $\theta_i = 87^0$) at $\lambda = 1.55$ μm, with the following grating parameters to achieve a broad spectral range of operation: $D = 730$ nm, $t_g = 1.04$ μm, duty cycle (ratio of grating width to period) $\eta = 65\%$, high index grating relative permittivity $\varepsilon_{rh} = 12.96$ (corresponding to a semiconductor material), surrounded by air. Fig. 4 shows the comparison between our results of the TE fundamental mode propagation loss of the waveguide as a function of wavelength obtained with (33) and those obtained in [5], where dielectric losses of the material

are negligible. In this figure it can be checked that both analysis methods yield identical results when negligible material absorption is assumed (which is a realistic assumption in the near infrared). However, it is worth mentioning that the propagation loss in this waveguide can be greatly dependent on such parameter, as we will see in the next example at THz frequencies.

C. PROPOSED DESIGN OF A THZ HOLLOW-CORE WAVEGUIDE USING SURFACE-RELIEF GRATINGS

We have taken advantage of the developed analysis method to design a realistic THz waveguide, in which the microstructure is not suspended in air as the one in Fig. 3, but properly supported by a slab of the same material. It is well known that material losses at such frequencies can not be neglected. Therefore, on the one hand, special attention must be paid when choosing the most appropriate configuration of a THz guidance system. And, on the other hand, there is need of using a rigorous method like the one presented in this work, in order to properly account for material losses. While other highly reflective structures, such as distributed Bragg reflectors (DBRs) or photonic crystals (PhCs), require multiple layers to achieve a high reflectivity, the HCG structure can achieve a very high field confinement in a hollow-core waveguide by using a single layer of cladding grating. Because of this, the field penetration depth in a HCG-HW cladding is significantly reduced compared to DBR or PhC based hollow-core waveguides, and consequently, its attenuation loss factor diminishes. In this case, surface-relief gratings have been chosen as high reflective structures for easy-of-fabrication purposes [25]. Thus, the proposed THz hollow-core waveguide consists of two reflecting surface-relief subwavelength gratings that are periodic in the z direction and infinite in the y direction (see the figure inset in Fig. 5). We have chosen our design frequency at 1.8 THz, and the selected high-index material is high-resistivity crystalline silicon, which, despite of a higher cost, is known to be an excellent dielectric material at terahertz frequencies [26]. The parameters of the grating are as follows: $D = 74\ \mu$m, $t_h = 50\mu$m, $t_p = 111\mu$m, duty cycle (ratio of grating width to period) $\eta = 50\%$, high index grating relative permittivity $\varepsilon_{rh} = 11.66$, $\tan\delta_h = 0.0002$, $a = 1610\ \mu$m. In Fig. 5 it is represented the reflectivity of this surface-relief grating under TE plane-wave incidence at the angle of the 0-iteration as a function of frequency. This reflectivity, which is related to the reflection coefficient ρ, represents the percentage of reflected power at each frequency under such angle of incidence, and it has been calculated following the procedure described in [16]. In this figure, it can be seen that the maximum reflectivity is achieved at 1.8 THz. The calculated reflection coefficient can also be related to the TE surface impedance Z_s^{TE} by using (31).

Following the iterative method described in Subsection III-A, the TE fundamental mode propagation loss of the designed THz waveguide has been calculated, including both reflection and material losses in the surface-relief

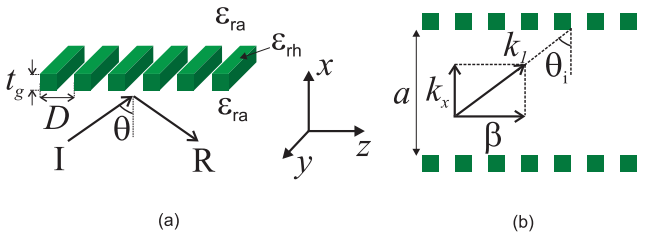

FIGURE 3. (a) Schematic of a high contrast grating (HCG) formed by high index material bars of ε_{rh} surrounded by a low index material, typically air (ε_{ra}). (b) Schematic of a hollow-core waveguide structure consisting of two reflecting HCGs.

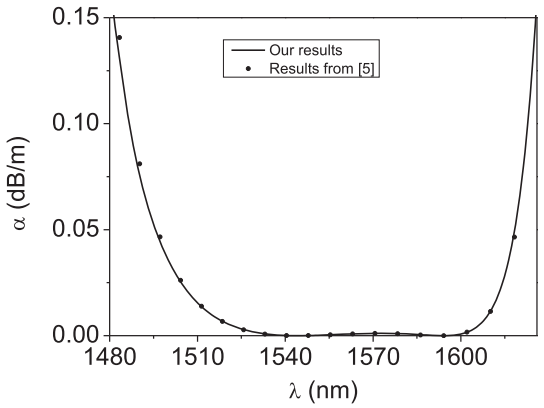

FIGURE 4. Comparison between our results of the TE fundamental mode propagation loss of the waveguide as a function of wavelength and those obtained in [5].

gratings constituting the waveguide walls. To this end, first of all, a convergence study of the obtained results with the iterative method has been performed with both the real and imaginary parts of Z_S and the propagation factor β at each frequency value. This analysis was performed with a sufficiently high number of iterations to guarantee that the results will not diverge again, revealing that only four iterations were needed for achieving the convergence, as it can be observed in Fig. 6 (in such figure, it is represented the normalized magnitudes $\mathrm{Re}(\overline{Z}_S)$ and $\mathrm{Im}(\overline{Z}_S)$ to the converged value, respectively, at such frequencies). It is worth mentioning that a similar convergence study for a much higher dielectric loss has shown to require a similar number of iterations for achieving the convergence of $\overline{Z}_s$, demonstrating the efficiency of this method. On the other hand, in Fig. 7 it can be observed the variation of the real and imaginary parts of Z_S as a function of frequency. In this figure, it can be checked that the real part of Z_S remains nearly constant and equal to zero in the frequency range from 1.76 to 1.81 THz, which is precisely the interval where the reflectivity of the surface-relief grating constituting the waveguide walls represented in Fig. 5 is high. Likewise, both the real and imaginary parts of Z_S have an almost zero value at the design frequency of 1.8 GHz, corresponding to the maximum of the reflectivity.

Fig. 8 shows the real propagation factor β of the TE fundamental mode of the designed waveguide at 1.8 THz obtained with the developed method (dashed line), and it

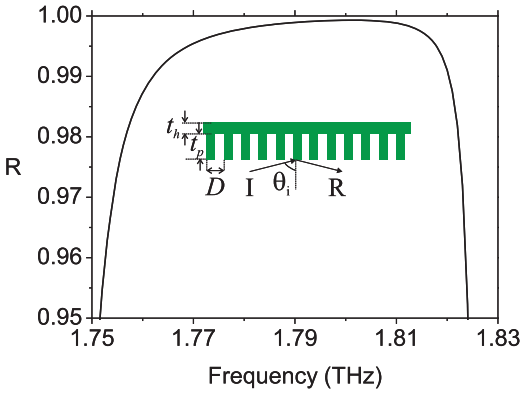

FIGURE 5. Reflectivity of the surface-relief grating employed in the THz hollow-core waveguide as a function of frequency.

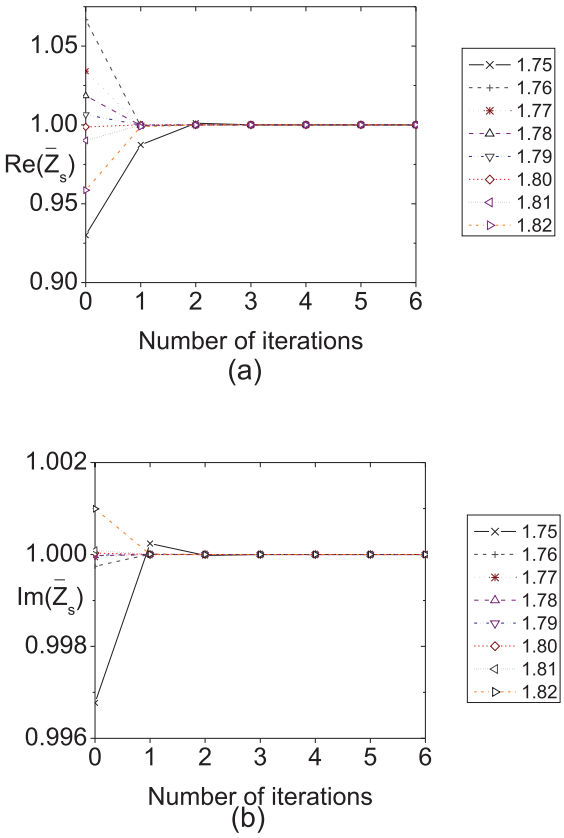

FIGURE 6. Convergence of the (a) real and (b) imaginary part of $\bar{Z}_S$ (normalized surface impedance to its converged value) at different frequency points (in THz).

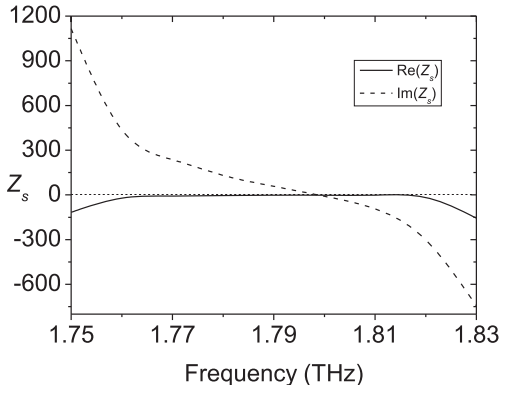

FIGURE 7. Variation of the real and imaginary parts of Z_S as a function of frequency.

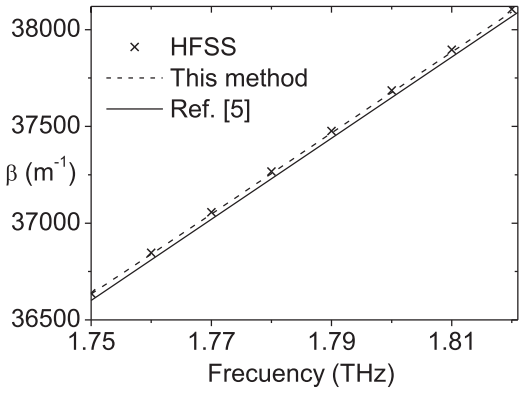

FIGURE 8. Real propagation factor of the TE fundamental mode of the designed THz waveguide as a function of frequency.

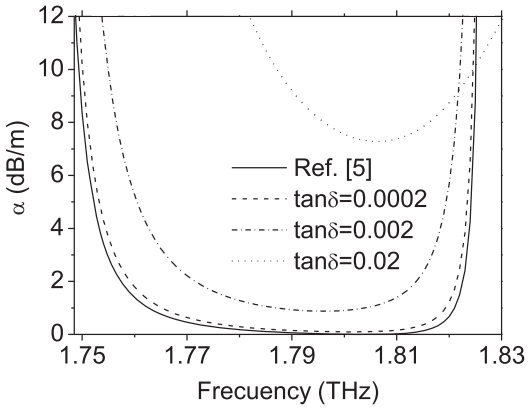

FIGURE 9. TE fundamental mode propagation loss of the designed THz waveguide as a function of frequency.

is compared with results provided by the commercial electromagnetic simulator HFSS (crosses) with the eigenmode solver, showing a perfect agreement (the driven modal solver failed to solve more than 25 modes, which was not enough to reach the desired mode). However, as explained in Section I, the eigenmode solver only provides the frequency behavior of the real part of the complex propagation factor of the propagating modes in the designed periodic hollow-core waveguide. More in detail, a unit cell of the waveguide defined by one period D surrounded by an air box with appropriate boundary conditions is analysed, including a sufficiently high number of modes in order to reach the mode we are interested in, which propagates in the air region delimited by

the dielectric gratings constituting the waveguide walls -i.e., with low propagation losses-. Thus, this comparison validates the obtained results. In this figure, it has also been included with solid line the real propagation factor obtained with the ray-optics approximation used in [5] for comparison, whose results are slightly different, as expected. Finally, in Fig. 9, the TE fundamental mode propagation loss of the designed THz waveguide as a function of frequency obtained with the ray-optics approximation [5] (solid line) is compared with that obtained with the surface-impedance formulation presented here, for different values of the loss tangent of the dielectric material, assuming no air propagation losses (this is a common assumption in hollow-core THz waveguides, in which air-filled THz devices are usually purged with nitrogen in order to avoid the possible wave attenuation associated to strong resonances of the H_2O molecules around 1.8 THz). These results show the importance of considering dielectric losses in this waveguide at THz frequencies. For the case of high-resistivity crystalline silicon ($\tan\delta_h = 0.0002$), this waveguide shows a very low propagation loss of 0.1 dB/m at the design frequency (although including the dielectric losses of the grating material), compared to other THz waveguides proposed in the technical literature [27], whereas a higher loss tangent of $\tan\delta_h = 0.02$ yields a significantly higher propagation loss (7.3 dB/m at 1.8 THz in this case). Thus, a special attention must be paid to the selection of the material to be employed in the implementation of the waveguide.

IV. CONCLUSION

A rigorous SI formulation for planar waveguides has been presented. This formulation provides a relatively simple, but rigorous, modal solution for planar waveguides defined by special boundary conditions, as it is the case of waveguides with subwavelength gratings or microstructured surfaces. Thus, any available numerical or analytical analysis of microstructured surfaces and special interfaces can be exploited to obtain the SI. Then, the modes can be obtained solving the characteristic equations, for example with an iterative method as the one reported here. The present formulation appears to have a high potential for the analysis of THz waveguides in which microstructured surfaces are commonly proposed to guide the electromagnetic waves, and require a full-wave vector analysis including material absorption and radiation losses. Future work can exploit the SI formulation, on the one hand, to model in the THz domain waveguides, couplers, and other components that are being developed in the optical domain using the concept of one-dimensional high-contrast metastructures [32], and, on the other hand, the extension of the present formulation to cylindrical symmetry, following the basic formulation reported in [14], will provide an interesting alternative for the study and design of THz cylindrical waveguides based on the antiresonant [3] and bandgap [4] concepts.

.

APPENDIX A CHARACTERISTIC EQUATIONS OF A PLANAR WAVEGUIDE IN TERMS OF THE SURFACE-IMPEDANCE ELEMENTS

In this appendix, there are shown the characteristic equations of a planar waveguide in terms of the SI elements. Such equations are:

$$\tan(k_x\frac{a}{2}) = \frac{(k_x^2\chi_{11}-k^2\chi_{22})-[(k_x^2\chi_{11}+k^2\chi_{22})^2+4k_x^2k^2\chi_{12}\chi_{21}]^{1/2}}{2k_x\omega\mu} \tag{A.34}$$

$$\tan(k_x\frac{a}{2}) = \frac{(k_x^2\chi_{11}+k^2\chi_{22})+[(k_x^2\chi_{11}-k^2\chi_{22})^2+4k_x^2k^2\chi_{12}\chi_{21}]^{1/2}}{2k_x\omega\varepsilon[\chi_{12}\chi_{21}-\chi_{11}\chi_{22}]} \tag{A.35}$$

$$\tan(k_x\frac{a}{2}) = \frac{(k_x^2\chi_{11}+k^2\chi_{22})-[(k_x^2\chi_{11}-k^2\chi_{22})^2+4k_x^2k^2\chi_{12}\chi_{21}]^{1/2}}{2k_x\omega\varepsilon[\chi_{12}\chi_{21}-\chi_{11}\chi_{22}]} \tag{A.36}$$

$$\tan(k_x\frac{a}{2}) = \frac{(k_x^2\chi_{11}+k^2\chi_{22})+[(k_x^2\chi_{11}-k^2\chi_{22})^2+4k_x^2k^2\chi_{12}\chi_{21}]^{1/2}}{2k_x\omega\mu} \tag{A.37}$$

where $k^2 = \omega^2\mu\varepsilon$.

APPENDIX B CALCULATION OF THE REFLECTION COEFFICIENT OF THE GRATING THAT CONSTITUTE THE HOLLOW-CORE WAVEGUIDE FOR PLANE WAVE INCIDENCE

Here it is briefly described how to obtain the reflection coefficient of a dielectric grating like the one defining the hollow-core waveguide under study in this work for plane wave incidence (see Figs. 3 or 5). To this end, the electromagnetic fields must be evaluated in all regions of the structure. Then, the general solutions are requested to satisfy the boundary conditions at the planar interfaces separating the constituent layers. Note that the coordinate reference system employed in this Appendix is different with respect to that in the main text: the periodicity D is chosen in the Y direction, being the grating homogeneous in the X axis. The grating is illuminated from the air region by an arbitrary linearly polarized plane wave which, in the most general case of 3D incidence (also called conical incidence), has a wave vector given by

$$\mathbf{k} = k_0\sin\theta\cos\phi\,\hat{\mathbf{x}} + k_0\sin\theta\sin\phi\,\hat{\mathbf{y}} + k_0\cos\theta\,\hat{\mathbf{z}}$$

where $k_0 = \omega\sqrt{\mu_0\varepsilon_0}$ is the wavenumber in free space, and θ and ϕ are the elevation and azimuthal angles of the three-dimensional incident plane wave, respectively. In order to obtain the modal spectrum in all regions of the structure,

the fields are assumed to have a harmonic time dependence, $exp\ (j\omega t)$, and since each region of the structure has translational symmetry in the Z direction, the propagating modes in this direction have an exponential dependence $exp\ (-j\beta z)$, where β is the modal propagation constant. Following [28], the modes in the homogeneous regions are the well known Floquet harmonics with E-type or TM^y polarization (denoted as $'$), and H-type or TE^y polarization (denoted as $''$) which are described as follows [29]

$$\begin{aligned}
\mathbf{e}_p^{'h} &= \frac{e^{-j(k_x x+k_{y_p} y)}}{\sqrt{D}\beta_{h_p}\omega\varepsilon_h}\left[-k_x k_{y_p}\widehat{\mathbf{x}} + (k_h^2 - k_{y_p}^2)\widehat{\mathbf{y}}\right] \\
\tilde{\mathbf{h}}_p^{'h} &= \frac{-e^{-j(k_x x+k_{y_p} y)}}{\sqrt{D}}\widehat{\mathbf{x}} \\
\tilde{\mathbf{e}}_p^{''h} &= \frac{\omega\mu\beta_{h_p}}{\sqrt{D}(k_h^2 - k_{y_p}^2)} e^{-j(k_x x+k_{y_p} y)}\widehat{\mathbf{x}} \\
\tilde{\mathbf{h}}_p^{''h} &= \frac{e^{-j(k_x x+k_{y_p} y)}}{\sqrt{D}}\left[\frac{-k_x k_{y_p}}{(k_h^2 - k_{y_p}^2)}\widehat{\mathbf{x}} + \widehat{\mathbf{y}}\right]
\end{aligned} \tag{B.38}$$

where $\varepsilon_h = \varepsilon_{rh}\varepsilon_0$ is the permittivity of the outer medium, $k_h = k_0\sqrt{\varepsilon_{rh}}$, $\beta_{h_p} = \sqrt{k_h^2 - k_x^2 - k_{y_p}^2}$, and k_{y_p} is the Floquet wavenumber given by

$$\begin{aligned}
k_{y_p} &= k_0 \sin\theta \sin\phi + \frac{2\pi}{D}p; \\
p &= 0, \pm 1, \pm 2, \ldots
\end{aligned} \tag{B.39}$$

Note that the geometry is homogeneous in the X direction, therefore $k_x = k_0 \sin\theta \cos\phi$.

The modes in the periodic region are obtained using a vectorial modal method [16], which has been extended for considering the three-dimensional incidence case [28]. In such method, the vector wave equation satisfied by the transverse components of the magnetic field in the periodic medium is expressed as an eigenvalue problem shown next

$$\begin{aligned}
&\left[\nabla_t^2 + k_0^2\varepsilon_r + \left(\frac{\nabla_t \varepsilon_r}{\varepsilon_r}\right) \times (\nabla_t \times \circ)\right]\mathbf{h} = \beta^2\mathbf{h} \\
&\Rightarrow L\mathbf{h}_n = \beta_n^2\mathbf{h}_n
\end{aligned} \tag{B.40}$$

where L represents the differential operator governing the evolution of the transverse magnetic field of the n-th mode along the Z axis, being β_n the modal propagation constant of such mode, and ε_r is the complex relative permittivity of the medium, which is a function depending on the transverse coordinates. Following the standard Method of Moments [30], this eigenvalue equation can be expressed in a matrix form if the modes in the periodic medium are expanded in terms of an auxiliary system whose eigenvectors satisfy an orthogonality relation of the form

$$\langle \tilde{\mathbf{e}}_p | \tilde{\mathbf{h}}_q \rangle = \delta_{pq}\ . \tag{B.41}$$

Thus, the modes of the real problem can be expanded in terms of the auxiliary system as

$$\mathbf{h_n} = \sum_q c_{qn}\tilde{\mathbf{h}}_q \tag{B.42}$$

where c_{qn} are the complex coefficients of the modal expansion for the transverse magnetic field of the n-th mode.

For the auxiliary basis we have used the modes corresponding to a homogeneous medium (B.38) of relative dielectric permittivity $\tilde{\varepsilon}_{rb}$, which has been adequately normalized for satisfying the following orthogonality relationship:

$$\langle \tilde{\mathbf{e}}_p | \tilde{\mathbf{h}}_q \rangle = \int_{CS} (\tilde{\mathbf{e}}_p^* \times \tilde{\mathbf{h}}_q) \cdot \widehat{\mathbf{z}} dS = \delta_{pq} \tag{B.43}$$

where CS represents in this case the cross section of the periodic cell. Then, the application of the Method of Moments yields the following linear matrix eigenvalue problem:

$$\sum_q L_{pq} c_{qn} = \beta_n^2 c_{pn} \tag{B.44}$$

where L_{pq} are the matrix elements of the L operator, which are obtained as follows:

$$L_{pq} = \langle \tilde{\mathbf{e}}_p | L\tilde{\mathbf{h}}_q \rangle = \int_{CS} (\tilde{\mathbf{e}}_p^* \times L\tilde{\mathbf{h}}_q) \cdot \widehat{\mathbf{z}} dS. \tag{B.45}$$

Note that the standard Galerkin's procedure has not been employed.

In the described theory, when all modes are included, the $[L]$ matrix is infinitely-dimensional. In order to develop a realistic method, a finite set of well-known auxiliary modes must be chosen to expand the modes of the periodic dielectric layer in terms of the modes of the auxiliary basis functions, so a numerical convergence test must be performed by sweeping the number of auxiliary modes over meaningful ranges, and then studying the stability of the numerical solutions provided by the algorithm.

The numerical diagonalization of (B.44) yields the propagation constants and the magnetic fields of the modes in the periodic medium at each frequency point. Finally, the transverse electric fields of the modes are related to the magnetic ones through constraints directly derived from Maxwell's equations [22], resulting

$$\mathbf{e}_n = \frac{j}{\omega\varepsilon}\widehat{\mathbf{z}} \times \left[\frac{1}{j\beta_n}\nabla_t[\nabla_t \cdot \mathbf{h}_n] + j\beta_n \mathbf{h}_n\right]. \tag{B.46}$$

For the particular case of 2D incidence ($\phi = 90^0$), the problem can be substantially reduced, given that there is no coupling between E-Type and H-Type Floquet modes, so the modes guided by the periodic medium are E-Type or H-Type modes, or equivalently, TM or TE modes, and thus, the TE and TM incidence cases can be analysed separately. Additionally, (B.46) is reduced to:

$$\mathbf{e}_n^{\mathrm{TE,TM}} = Z_n^{\mathrm{TE,TM}}(\mathbf{h}_n^{\mathrm{TE,TM}} \times \mathbf{z}). \tag{B.47}$$

After specifying the fields in all regions of the structure, both homogeneous and periodic, the problem is reduced to obtain the scattering parameters of the structure. To this end, the boundary conditions between adjacent layers will be imposed, obtaining the generalized scattering matrix (GSM) at each interface between adjacent layers of the structure, i.e., the amplitudes of reflected and transmitted modes. Then,

we construct the GSM of the global structure by means of the cascaded connection of the individual GSMs of the interfaces and the scattering matrices corresponding to the propagation through the layers, following the technique described in [31]. The global GSM yields the amplitudes of the scattered modes, which are reflected and transmitted by the structure, considering an incident plane wave with a unit amplitude.

Finally, we have to consider that the multimode scattering matrix is infinitely-dimensional. In order to reduce the scattering problem to a computationally tractable form, the individual multimode scattering matrices should be reduced at a finite size. Such a size must be large enough to allow for accurate calculation of the scattered modes which are significant in the overall solution, but at the same time small enough for efficient numerical calculation. Then, for each particular case, a study of convergence must be performed in order to reach an accurate solution for both the propagation characteristics in each periodic layer, and the scattering parameters of the overall structure.

REFERENCES

[1] G. Gallot, S. P. Jamison, R. W. McGowan, and D. Grischkowsky, "Terahertz waveguides," *J. Opt. Soc. Amer. B*, vol. 17, no. 5, pp. 851–863, May 2000, doi: 10.1364/JOSAB.17.000851.

[2] Y. Zhou, M. C. Y. Huang, C. Chase, V. Karagodsky, M. Moewe, B. Pesala, F. G. Sedgwick, and C. J. Chang-Hasnain, "High-index-contrast grating (HCG) and its applications in optoelectronic devices," *IEEE J. Sel. Topics Quantum Electron.*, vol. 15, no. 5, pp. 1485–1499, Sep. 2009, doi: 10.1109/JSTQE.2009.2021145.

[3] H. Bao, K. Nielsen, O. Bang, and P. U. Jepsen, "Dielectric tube waveguides with absorptive cladding for broadband, low-dispersion and low loss THz guiding," *Sci. Rep.*, vol. 5, no. 1, p. 7620, Jan. 2015, doi: 10.1038/srep07620.

[4] K. Nielsen, H. K. Rasmussen, A. J. L. Adam, P. C. M. Planken, O. Bang, and P. U. Jepsen, "Bendable, low-loss Topas fibers for the terahertz frequency range," *Opt. Exp.*, vol. 17, no. 10, pp. 8592–8601, May 2009, doi: 10.1364/OE.17.008592.

[5] Y. Zhou, V. Karagodsky, B. Pesala, F. G. Sedgwick, and C. J. Chang-Hasnain, "A novel ultra-low loss hollow-core waveguide using subwavelength high-contrast gratings," *Opt. Exp.*, vol. 17, no. 3, pp. 1508–1517, 2009, doi: 10.1364/OE.17.001508.

[6] V. Karagodsky, B. Pesala, F. G. Sedgwick, and C. J. Chang-Hasnain, "Dispersion properties of high-contrast grating hollow-core waveguides," *Opt. Lett.*, vol. 35, no. 24, pp. 4099–4101, Dec. 2010, doi: 10.1364/OL.35.004099.

[7] V. Setti, L. Vincetti, and A. Argyros, "Flexible tube lattice fibers for terahertz applications," *Opt. Exp.*, vol. 21, no. 3, pp. 3388–3399, Feb. 2013, doi: 10.1364/OE.21.003388.

[8] S. Atakaramians, S. Afshar, H. Ebendorff-Heidepriem, M. Nagel, B. M. Fischer, D. Abbott, and T. M. Monro, "THz porous fibers: Design, fabrication and experimental characterization," *Opt. Exp.*, vol. 17, no. 16, pp. 14053–14062, Jul. 2009, doi: 10.1364/OE.17.014053.

[9] A. Hassani, A. Dupuis, and M. Skorobogatiy, "Porous polymer fibers for low-loss terahertz guiding," *Opt. Exp.*, vol. 16, no. 9, pp. 6340–6351, 2008, doi: 10.1364/OE.16.006340.

[10] (2020). *CST Microwave Studio*. Accessed: Dec. 2020. [Online]. Available: https://www.cst.com/products/cstmws

[11] *ANSYS High Frequency Structure Simulator (HFSS)*. Accessed: Dec. 2020. [Online]. Available: https://www.ansys.com/products/ electronics/ansys-hfss

[12] J. Martínez, A. Coves, F. Mesa, and O. Quevedo-Teruel, "Passband broadening of sub-wavelength resonator-based glide-symmetric SIW filters," *AEU-Int. J. Electron. Commun.*, vol. 125, Oct. 2020, Art. no. 153362, doi: 10.1016/j.aeue.2020.153362.

[13] H. M. Barlow and A. L. Cullen, "Surface waves," *Proc. IRE*, vol. 100, no. 16, pp. 329–347, 1953.

[14] J. Y. Savard, "Higher-order cylindrical surface-wave modes," *IEEE Trans. Microw. Theory Techn.*, vol. 15, no. 3, pp. 151–155, Mar. 1967, doi: 10.1109/TMTT.1967.1126404.

[15] D. Lu, M. Wan, Z. Li, S. Huang, W. Zhang, B. Li, X. Lu, X. Li, and X. Fang, "Photonic bandgap terahertz fibers based on honeycombed tubes," *Opt. Exp.*, vol. 29, no. 26, pp. 43516–43530, 2021, doi: 10.1364/OE.433608.

[16] A. Coves, B. Gimeno, J. Gil, M. V. Andres, A. A. S. Blas, and V. E. Boria, "Full-wave analysis of dielectric frequency-selective surfaces using a vectorial modal method," *IEEE Trans. Antennas Propag.*, vol. 52, no. 8, pp. 2091–2099, Aug. 2004, doi: 10.1109/TAP.2004.832507.

[17] F. Mesa, G. Valerio, R. Rodriguez-Berral, and O. Quevedo-Teruel, "Simulation-assisted efficient computation of the dispersion diagram of periodic structures: A comprehensive overview with applications to filters, leaky-wave antennas and metasurfaces," *IEEE Antennas Propag. Mag.*, vol. 63, no. 5, pp. 33–45, Oct. 2021, doi: 10.1109/MAP.2020.3003210.

[18] Q. Chen, F. Mesa, X. Yin, and O. Quevedo-Teruel, "Accurate characterization and design guidelines of glide-symmetric holey EBG," *IEEE Trans. Microw. Theory Techn.*, vol. 68, no. 12, pp. 4984–4994, Dec. 2020, doi: 10.1109/TMTT.2020.3023751.

[19] H. A. Macleod, *Thin-Film Optical Filters*. Bristol, U.K.: Adam Hilger, 1986.

[20] R.-S. Chu and K.-M. Lee, "Analytical method of a multilayered meander-line polarizer plate with normal and oblique plane-wave incidence," *IEEE Trans. Antennas Propag.*, vol. 35, no. 6, pp. 652–661, Jun. 1987, doi: 10.1109/TAP.1987.1144158.

[21] M. David Pozar, *Microwave Engineering*. Hoboken, NJ, USA: Wiley, 2012.

[22] E. Robert Collin, *Field Theory Guided Waves*. Hoboken, NJ, USA: Wiley, 1990.

[23] H. A. Haus, *Waves and Fields in Optoelectronics* (Series in Solid State Physical Electronics). Upper Saddle River, NJ, USA: Prentice-Hall, 1984.

[24] E. Silvestre, M. A. Abian, B. Gimeno, A. Ferrando, M. V. Andres, and V. E. Boria, "Analysis of inhomogeneously filled waveguides using a bi-orthonormal-basis method," *IEEE Trans. Microw. Theory Techn.*, vol. 48, no. 4, pp. 589–596, Apr. 2000, doi: 10.1109/22.842031.

[25] Á. Coves, B. Gimeno, and M. V. Andrés, "Oblique incidence and polarization effects in coupled gratings," *Opt. Exp.*, vol. 20, no. 23, pp. 25454–25460, Nov. 2012, doi: 10.1364/OE.20.025454.

[26] P. H. Bolivar, M. Brucherseifer, J. Gómez, R. Gonzalo, I. Ederra, A. L. Reynolds, M. Holker, and P. de Maagt, "Measurement of the dielectric constant and loss tangent of high dielectric-constant materials at terahertz frequencies," *IEEE Trans. Microw. Theory Techn.*, vol. 51, no. 4, pp. 1062–1066, Apr. 2003, doi: 10.1109/TMTT.2003.809693.

[27] S. Atakaramians, S. Afshar V., T. M. Monro, and D. Abbott, "Terahertz dielectric waveguides," *Adv. Opt. Photon.*, vol. 5, no. 2, pp. 169–215, Jun. 2013, doi: 10.1364/AOP.5.000169.

[28] A. Coves, B. Gimeno, A. A. S. Blas, A. Vidal, V. E. Boria, and M. V. Andres, "Three-dimensional scattering of dielectric gratings under plane-wave excitation," *IEEE Antennas Wireless Propag. Lett.*, vol. 2, pp. 215–218, 2003.

[29] H. M. Altschuler and L. O. Goldstone, "On network representations of certain obstacles in waveguide regions," *IRE Trans. Microw. Theory Techn.*, vol. 7, no. 2, pp. 213–221, 1959.

[30] R. F. Harrington, *Field Computation by Moment Methods*. Piscataway, NJ, USA: IEEE Press, 1993.

[31] T. S. Chu and T. Itoh, "Generalized scattering matrix method for analysis of cascaded and offset microstrip step discontinuities," *IEEE Trans. Microw. Theory Techn.*, vol. 34, no. 2, pp. 280–284, Feb. 1986, doi: 10.1109/TMTT.1986.1133323.

[32] P. Qiao, W. Yang, and C. J. Chang-Hasnain, "Recent advances in high-contrast metastructures, metasurfaces, and photonic crystals," *Adv. Opt. Photon.*, vol. 10, no. 1, pp. 180–245, 2018, doi: 10.1364/AOP.10.000180.

ANGELA COVES (Senior Member, IEEE) received the Licenciado and Ph.D. degrees in physics from the University of Valencia, Spain, in 1999 and 2004, respectively.

She is currently a Professor with the Department of Communications Engineering, Universidad Miguel Hernández de Elche, Spain. Her research interests include microwave passive components, RF breakdown high-power effects, and waveguide theory.

HAROLDO MAESTRE received the M.S. and Ph.D. degrees in electrical engineering from Universidad Miguel Hernández, Elche, Spain, in 2005 and 2011, respectively.

From 2008 to 2009, he was with the Ultrashort Spectroscopy and THz Physics Group, Johann Wolfgang Goethe Universität, Frankfurt am Main, Germany, working on nonlinear mixers for THz photonic generation. He has been an Associate Professor at the Universidad Miguel Hernández de Elche, since 2019. His current research interests include microwave photonics, solid-state lasers, and nonlinear optical frequency conversion for communication and imaging systems applications.

RAIMON ARCHILÉS was born in Castellón, Spain, in 1989. He graduated in physics from the University of Valencia, in 2015. He received the master's degree in advanced physics with a speciality in photonics from the University of Valencia, in 2017.

MIGUEL V. ANDRÉS (Senior Member, IEEE) received the B.Sc. and Ph.D. degrees in physics from the University of Valencia, Spain, in 1979 and 1985, respectively.

After a postdoctoral stay (1984–1987) at the Department of Physics, University of Surrey, U.K., he founded the Group of Fiber Optics, University of Valencia. He is currently a Professor of applied physics at the University of Valencia and responsible for the leadership and management of the Group of Fiber Optics, University of Valencia. His research activity includes an increasing number of collaborations with Latin–American universities and research institutes of Mexico, Argentina, Costa Rica, Peru, and among others. His current research interests include photonic crystal fibers, in-fiber acousto-optics, fiber lasers and new fiber-based light sources, fiber sensors, microwave photonics, and waveguide theory.

BENITO GIMENO (Member, IEEE) received the Licenciado degree in physics and the Ph.D. degree from the University of Valencia, Valencia, Spain, in 1987 and 1992, respectively.

He became a Full Professor at the University of Valencia, in 2010. His current research interests include the electromagnetic analysis and design of microwave passive components and RF breakdown high-power effects.